ORIGINAL ARTICLE

Nephroprotective properties of chitosan/sodium lignosulfonate/Au nanoparticles in streptozotocin-induced nephropathy in mice: Introducing a novel therapeutic drug for the treatment of nephropathy

Yimeng Gong [a,1], Xiaoyun Guo [b,1], Qihan Zhu [c,*]

[a] *Department of Nephrology, Sichuan Second Hospital of TCM, Sichuan 610031, China*
[b] *Department of Nephrology, The Second Hospital of Tianjin Medical University, Tianjin 300211, China*
[c] *Departments of Endocrinology, The First Affiliated Hospital of Wenzhou Medical University, Zhejiang 325000, China*

Abstract In this study, we report the green synthesis of nontoxic, stable, and small size gold nanoparticle by using chitosan/sodium lignosulfonate hydrogel with capping/reducing ability for the synthesis of CS/NaLS/Au NPs. The prepared bio-nanocomposite were characterized by advanced physicochemical techniques like Scanning Electron Microscopy (SEM), Transmission Electron Microscopy (TEM), Energy Dispersive X-ray spectroscopy (EDX) and X-ray Diffraction (XRD) study. It has been established that CS/NaLS/Au NPs have a spherical shape with a mean diameter from 20 to 30 nm. Diabetes was induced by administration of 60 mg/kg of streptozotocin (STZ) intraperitoneally in 100 mature male mice and they were randomly divided into 5 groups. The negative control group received normal saline and treatment groups received glibenclamide with dose 0.5 mg/kg and 10 and 40 μg/kg of CS/NaLS/Au NPs through gavage for 50 days. In addition, one group considered as positive control (in treated-diabetic). On the last day, serum levels of samples blood glucose, urea and creatinine were measured. After tissue processing, 5 μm sections of the kidneys were prepared and they were stained by periodic acid Schiff (PAS) and used for stereological analysis. In the antioxidant test, the IC50 of CS/NaLS/Au NPs and BHT against DPPH free radicals were 117 and 86 μg/mL, respectively. In the cellular and molecular part of the recent study, the treated cells with CS/NaLS/Au NPs were assessed by MTT assay for 48 h about the cytotoxicity properties on normal (HUVEC) cell line. The increased levels of blood glucose and urea were

* Corresponding author.
 E-mail address: zhuqihandoc@126.com (Q. Zhu).
[1] Yimeng Gong and Xiaoyun Guo contributed equally to this research and should be considered co-first authors.

decreased ($p < 0.05$) significantly in CS/NaLS/Au NPs-treated groups as compared to the untreated diabetic. The kidney weight, kidney volume (Volume of cortex, medulla, glomerulus, proximal and distal tubules, collecting ducts, loop of Henle, interstitial tissues, and vessels) and kidney structures length (length of proximal and distal tubules, collecting ducts, loop of Henle, and vessels) decreased significantly ($p < 0.05$) after treatment with high dose of CS/NaLS/Au NPs ($p < 0.05$). According to the obtained results, CS/NaLS/Au NPs can regulates the levels of blood glucose and urea and inhibits from kidney damages in STZ-induced diabetic mice. This study suggested CS/NaLS/Au NPs as an antidiabetic and nephroprotective drug in the developing countries.

1. Introduction

Diabetic nephropathy or diabetic kidney disease is a syndrome characterized by the presence of pathological quantities of urine albumin excretion, diabetic glomerular lesions, and loss of glomerular filtration rate in diabetics (International Diabetes Federation, 2013; Centers for Disease Control and Prevention, 2011; Tapp et al., 2004). Diabetes may be classified as type 1 (autoimmune β-cell destruction and absolute insulin deficiency), type 2 (relative insulin deficiency and resistance), and other types (e.g., pancreatic disease). Not all diabetics develop diabetic nephropathy and in those who do, progression is variable (Tapp et al., 2004; Scott et al., 2001; Rossing et al., 2002; Satko et al., 2002). The main modifiable risks are hypertension, glycemic control, and dyslipidemia. Data from the Joslin Diabetes Center, Steno Diabetes Center, and AusDiab studies also strongly implicate smoking as a risk factor for diabetic nephropathy (Tapp et al., 2004; Scott et al., 2001; Rossing et al., 2002). The main unmodifiable risks are age, race, and genetic profile. Diabetic nephropathy is more likely to develop in patients with a family history of diabetic nephropathy (Satko et al., 2002; Pettitt et al., 1990; Seaquist et al., 1989). Certain racial groups are also at higher risk, such as African Americans, Mexican Americans, and Pima Indians (Seaquist et al., 1989; Young et al., 2003). One study suggested that males had an increased risk of diabetic nephropathy (Young et al., 2003; Smith et al., 1991). A meta-analysis of studies identified 24 genetic variants in 16 genes which are associated with diabetic nephropathy. These include *ACE*; *ALR2*; *APOC1*, *APOE*, *EPO*, *eNOS*, *HSPG2*, *VEGF*, *FRMD3*, *CARS*, *UNC13B*, *CPVL/CHN2*, and *GREM1*. In a subgroup of type 2 diabetic Asians, *ELMO1*, *CCR5*, and *CNDP1* were also relevant (Pettitt et al., 1990; Seaquist et al., 1989; Young et al., 2003). Other meta-analyses implicated polymorphisms of *ADIPOQ*; *PAI-1*, *TGFβ1*, and *PPARγ* in the development of diabetic nephropathy. The nature of the polymorphism varies with ethnicity (Satko et al., 2002; Pettitt et al., 1990; Seaquist et al., 1989; Young et al., 2003). The complexity of genetic studies in diabetic nephropathy is discussed in a review by Mooyaart (Satko et al., 2002; Pettitt et al., 1990). Treatment to delay diabetic nephropathy progression involves adequate control of metabolic and hemodynamic abnormalities. In practical terms, this means adequate blood glucose lowering and control of hypertension (Pettitt et al., 1990; Seaquist et al., 1989; Young et al., 2003; Smith et al., 1991). Certain antihypertensives are also preferred based on studies, which have demonstrated reductions in proteinuria or preservation of GFR, or both. Nonpharmacological approaches and alternative medicine are briefly discussed. There is also interest in novel agents, gene therapy, and stem cell treatment, which may someday find a place in the treatment armamentarium (Satko et al., 2002; Pettitt et al., 1990; Seaquist et al., 1989; Young et al., 2003; Smith et al., 1991). In the recent years, the scientists have used the nanoparticles in the treatment of several diseases such as nephropathy (Torchilin, 2007; Itani and Al Faraj, 2019; Trojer et al., 2013; Miller and Krochta, 1997; Debeaufort et al., 1998).

Nanotechnology is defined in different ways in several countries, which affects the nanodrugs clinical validation. However, what these different definitions have in common is the use of nanoscale structures. There are several distinct benefits to using nanotechnology in the diseases treatment (Torchilin, 2007; Itani and Al Faraj, 2019). Nanoparticles, especially metal nanoparticles and metal oxides, have been widely used by medical consumers and manufacturers. The mechanism of nanoparticle-induced toxicity against abnormal cells is the production of reactive oxygen species (ROS). Excessive production of reactive oxygen species can lead to oxidative stress, disruption of normal physiological maintenance, and oxidation regulation. These effects in turn lead to DNA damage, unregulated cell signaling pathways, changes in cell evolution, cytotoxicity, apoptotic death, and the onset of cell death (Torchilin, 2007; Itani and Al Faraj, 2019; Trojer et al., 2013; Miller and Krochta, 1997).

Critical-deterministic factors can affect the production of reactive oxygen species. These critical-deterministic factors include shape, size, nanoparticle surface area, particle surface baroelectricity, surface-forming groups, Particle solubility, metal ion emission from nanomaterials and nanoparticles, optical activation, model of cell reactions, inflammatory effects and ambient pH (Smith et al., 1991; Torchilin, 2007; Itani and Al Faraj, 2019; Trojer et al., 2013; Miller and Krochta, 1997; Debeaufort et al., 1998). Metal nanoparticles and oxides of metal nanoparticles due to their optical properties due to the large active area and high atomic number, amplify the photoelectric and Compton effects of both X-ray and gamma-ray interactions with the adsorbent in the diagnostic and therapeutic range. Finally, they can lead to the development of methods for the destruction of tumor cells and reduce their survival with minimal side effects in radiation therapy (Trojer et al., 2013; Miller and Krochta, 1997; Debeaufort et al., 1998; Fazaeli et al., 2010; Xue et al., 2021). As a result, increasing industrial knowledge in the field of scalable nanoparticle synthesis, along with the design of multifunctional nanoparticles, will dramatically change the strategies of microenvironmental preparation and therapeutic-diagnostic nanoparticles for the treatment of several diseases (Itani and Al Faraj, 2019; Trojer et al., 2013; Miller and Krochta, 1997; Debeaufort et al., 1998).

In recent days, biomolecular engineered nanoparticles have come into prominence as novel formulated nanomedicine due to their excellent biocompatibility, small size to overcome the cell barrier, large surface area to carry the effective drug with high loading and selective targeting the drug to the affected area. There are ample reports on plant phytochemicals or biopolymer adorned nanoparticles being deployed in medicinal therapeutics (Trojer et al., 2013; Miller and Krochta, 1997; Debeaufort et al., 1998; Fazaeli et al., 2010; Xue et al., 2021; Shi et al., 2021; Huang et al., 2021; Zhao et al., 2021; Oueslati et al., 2020; Venditti, 2019; Rossi et al., 2016; Umamaheswari et al., 2018; Fratoddi et al., 2018; Aromal and Philip, 2012; Zhang et al., 2020; Shahriari et al., 2021). Among the different metal variants, Au NPs have been observed to demonstrate significant bioactivities as antioxidant, antifungal and antibacterial

properties over diverse fungi and bacteria (Zhaleh et al., 2019). They have also been explored to have significant potential in diseases diagnosis and as non-conventional chemotherapeutic drug both *in vitro* and *in vivo* studies (Sun et al., 2019; Wu et al., 2018; Ledari et al., 2020). Modified and bio-functionalized Au NPs have previously been reported to show stupendous consequences following *in-vitro* studies against a wide range of cancer cell lines like LL2, MCF-7/ADR, A549, H460, H520, HT29, HCT15, HCT116, RKO, U87, LN229, HeLa, HDF, C0045C, HepG2-R, Vero, 4 T1 and so on (Singh et al., 2018). These inputs have encouraged us to develop a novel nanocomposite material where *in situ* prepared Au NPs have been fabricated with two biomolecules chitosan and sodium lignosulphonate to shape it as a core-shell like appearance. These two molecules contain plenteous electron rich functional groups which facilitate the green reduction of Au ions to corresponding NPs without involving toxic chemicals. The dual biomolecular coatings also provide significant stability to the Au NPs by capping it, thereby preventing from agglomeration. The as-synthesized nanocomposite material has been characterized with different physicochemical techniques and subsequently applied as a therapeutic drug against streptozotocin-induced nephropathy in mice.

2. Experimental

2.1. Materials and method

The essential chemicals and biosamples were procured from Fluka and Sigma-Aldrich. All the reagents were used directly without any further purifications. In the structural characterizations, FT-IR was recorded over KBr disc in a Bruker VERTEX 80v spectrophotometer. The gas adsorption-desorption isotherms were carried out in a NOVA gas sorption analyzer and a Quantochrome BET surface area analyzer. Morphological and compositional analysis was done over FE-SEM MIRA3 microscope equipped with EDX (TSCAN). The samples were coated with gold atom vapor prior to analysis. A Philips CM10 microscope was used in the TEM analysis, performed at 200 kV operating voltage. The sample was prepared by dispersing it on a carbon coated Cu grid followed by drying. In the analysis of crystallinity, X-ray diffraction study was performed using Co Kα radiation (λ = 1.78897 Å, voltage 40 keV, current 40 mA) in the scanning range of 2θ = 10 to 80°. A STAT FAX 2100, BioTek, Winooski, USA instrument was used in Microplate Reading.

2.2. Preparation of the CS/NaLS/Au nanocomposite

A mixture of chitosan (CS, 98% NH_2) and sodium lignosulfonate (NaLS) (0.2 g each) were dissolved in100 mL of 1% (v/v) acetic acid solution by sonication for 30 min. It was then stirred overnight at room temperature to obtain the CS/NaLS composite hydrogel. In this stage pH of the solution was adjusted to pH 9 by alkali treatment (NaOH, 3 wt%) and subsequently an aqueous solution of $HAuCl_4$ (20 mg in 10 ml) was added drop-wise over a period of 10 min. The mixture was mechanically stirred for 2 h at 80 °C. The progress of the reaction could be monitored by change in solution color from watery yellow to dark-red, attributed to the excitation of the surface Plasmon resonance (SPR) band. This visual change is also an indication for the formation of Au NPs. The prepared CS/NaLS/Au nanocomposite were collected by centrifugation and washed several times with DI-water. According to ICP-OES analysis the gold content was 0.091 mmol/g.

2.3. Antioxidant activities of CS/NaLS/Au nanocomposite

In this method, 1 ml of different concentrations of the nanoparticles (0–1000 μg/ml) (with 1 ml of DPPH (300 μmol/l) combined and then the final volume of the combination with methanol reached 4000 μl. The falcons were then vertexed and kept in the dark for 60 min. The absorbance was read at 517 nm. The DPPH radical inhibition percentage was calculated using the following equation (Lu et al., 2021):

$$\text{Inhibition}(\%) = \frac{\text{Sample A.}}{\text{Control A.}} \times 100$$

2.4. Cytotoxicity properties of CS/NaLS/Au nano bio-composite

HUVEC or normal cells were used to evaluate the cytotoxicity effect of CS/NaLS/Au nano bio-composite on cell culture.

The HUVEC cells in DMEM culture medium (Gibco, USA) with 10% FBS (Gibco, USA) and penicillin / streptomycin (100 μl / 100 μg / ml) in an incubator containing 5% Carbon dioxide with 90% humidity was stored at 37 °C. Then, when about 80% of the flask was filled, cell passage was performed and about 5×10^4 cells (per square centimeter) were placed in 24 house bacterial petri dishes in the usual environment. The cells were treated with different concentrations of nanoparticles 24 h later and kept in this condition for 3 days. The survival rate of cultured cells was prepared with different concentrations. In this experiment, cells were cultured at 3×10^4 cells/well in 24-well plates and kept in an incubator at 37 °C for 24 h. Then the old culture medium was taken out of the wells and the cells were treated with different concentrations of nanoxidro. This test was performed on the first, second and third days after exposing the cells to the compounds; thus, at the appropriate time after culturing the cells in plates of 24 cells, the culture medium was removed and about 300 μl of fresh medium containing 30 μl of MTT solution was added to each cell. After 3–4 h of incubation at 37° C, MTT solution is removed and 200 μl (Dimethyl Sulfoxide, Merck, USA, 100%) DMSO is added to each house. Then the sample absorption was read at 570 wavelengths using ELISA rider (Expert 96, Asys Hitch, Ec Austria). This experiment was repeated 3 times and each time, four wells were considered for each nano oxide concentration. Cell survival percentage was evaluated by the following formula (Lu et al., 2021):

$$\text{Cell viability}(\%) = \frac{\text{Sample A.}}{\text{Control A.}} \times 100$$

2.5. In vivo design

2.5.1. Animals

One hundred male Balb/c mice weighing between 38 and 40 g were housed in an air-conditioned room (22 ± 2 °C) and had free access to the standard pellet diet and water ad libitum conditions during the study.

2.5.2. Experimental design

Diabetes was experimentally induced by intraperitoneal injection of STZ (60 mg/kg) in 80 mice. Fasting blood glucose levels were assessed everyday by glucometer strips. After three days, the mice with plasma glucose level > 250 mg/dL were consid-

ered diabetic. The mice were divided into five following groups ($n = 10$): I. Control group (C); II. Untreated-diabetic group; III. Treated group with 0.5 mg/kg glibenclamide (G30); IV. Treated group with 10 mg/kg of the CS/NaLS/Au NPs (CS/NaLS/Au NPs 10); V. Treated group with 40 mg/kg of the CS/NaLS/Au NPs (CS/NaLS/Au NPs 40). Blood samples were obtained in 0, 7, 13, 20 days from tail vein to assess the blood glucose level by Easy Gluco glucometer (Ames, Korea). Twenty three days after diabetes induction and at the end of the 20th day of the treatment, the animals of all groups were euthanized by ketamine HCl (40 mg/kg). Immediately, blood samples were drawn from mice heart and inserted in serum tubes for determination of urea and creatinine (Hagh-Nazari et al., 2017).

2.5.3. Histological study

2.5.3.1. Volume density.
After dissection, the left kidney was weighed then fixed in 10% neutral buffered formalin solution for one week. Immersion method was used to evaluate the kidney primary volume. For assessment of kidney final volume, the amount of tissue shrinkage must be determined (Braendgaard and Gundersen, 1986; Gundersen et al., 1992). The sections of organ were prepared using the orientator method. Totally, 7–10 slab were obtained from kidney. A circular piece was sampled from a kidney slab and the area of this piece was calculated. The slabs and circular piece were processed, sectioned (5 μm thicknesses) and stained by Periodic Acid Schiff (PAS) method. The area of the circular piece was calculated again and tissue shrinkage was measured (Mandarim-de-Lacerda, 2003):

$$\text{Volume shrinkage} = 1 - (\text{AA/AB})^{1.5}$$

AA and AB: The area of the circular piece after and before tissue processing.

The total volume of the organ was then estimated using:

$$V_{final} = V_{primary} \times (1 - \text{Volume shrinkage})$$

Tissue sections were examined using a video microscopy system. The fractional volume of the renal structures was measured using a point probe (with an area of 100 cm^2 and containing 25 points) and following formula:

$$V_v = P_{structure}/P_{reference}$$

$P_{structure}$ = sum of points hitting to the interested structures
$P_{reference}$ = sum of points hitting to the reference space

2.5.3.2. Length density.
The length density of the tubules and vessels was evaluated using an unbiased counting probe (740 × 740 μm). The length density was estimated as (Mandarim-de-Lacerda, 2003):

$$L_v = 2 \times \sum Q/a(\text{frame}) \times \sum \text{frame}$$

$\sum Q$ = sum of the tubules counted, a (frame) = probe area, 547,600 μm^2, $\sum$frame = total number of the counted frames.

All data were analyzed by Duncan's test of one-way variance analysis (ANOVA), using the SPSS 22 software package. Data were considered statistically significant at $p < 0.05$.

3. Results and discussion

3.1. Structural characterization of synthesized CS/NaLS/Au nanocomposite

A post-synthetic modification approach was followed in the strategically developed CS/NaLS/Au nanocomposite. It was based on preparation of a hydrogel by two biopolymers, CS and NaLS, which was subsequently exploited for *in situ* synthesis of Au NPs following green process. The final CS/
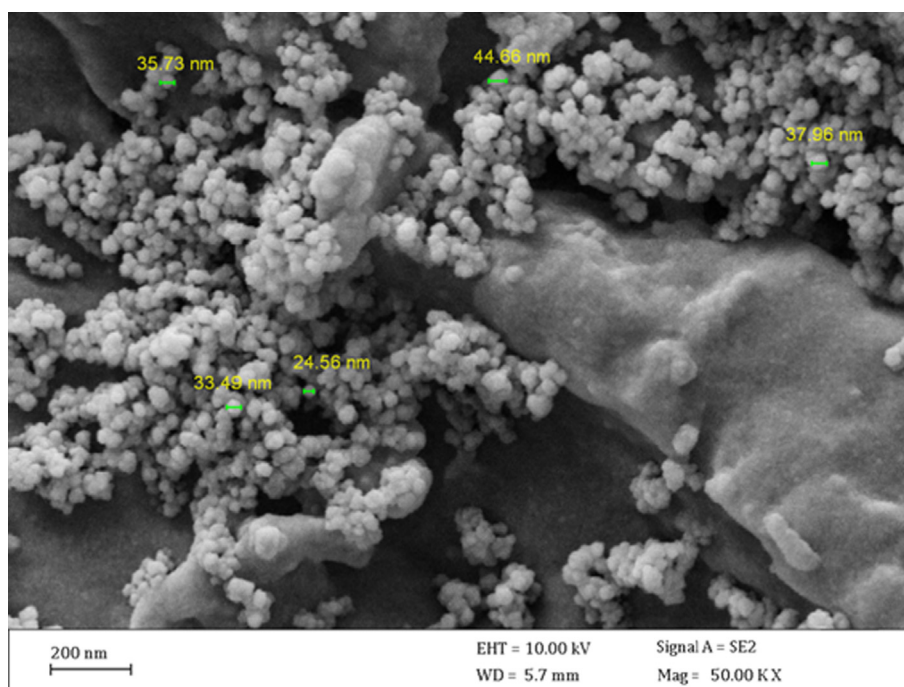

Fig. 1   FE-SEM image of the CS/NaLS/Au nanocomposite.

NaLS/Au nanocomposite was subsequently analyzed through several techniques, such as, SEM, TEM, EDX, XRD and ICP-OES.

The structural morphology, size and shape of the CS/NaLS/Au as synthesized nanocomposite was ascertained by FE-SEM and TEM analysis. Fig. 1 depicts the Fe-SEM image of the molecule. Evidently, the morphology is different from what we predicted the nanocomposite to be of core-shell structure. The small round shaped white granules represent the Au NPs which are spread over the CS-NaLS hydrogel composite. Average particle sizes of Au NPs lie between 25 and 35 nm. The Au NPs shows the impression to be aggregated to some extent, due to manual preparation of sample during analysis. More comprehensive structural assessment could be done from TEM analysis, as displayed in Fig. 2. The black dots, corresponding to Au NPs are homogeneously dispersed all over the surface in a pool of CS-NaLS composite hydrogel. They are well separated from each other and no sign of agglomeration is evidenced. Particle size of Au NPs are in close agreement to SEM analysis, around 30–35 nm.

Chemical composition of the CS/NaLS/Au nanocomposite was determined from EDX analysis and the corresponding profile is depicted in Fig. 3. It displays a major and distinct Au signal observed at 2.1 keV, characteristic of Au NP. In the lower region some small and weak signals of C, N and O are also observed, which are attributed to the CS and NaLS

hydrogel composite, thus validating their attachment and the anticipated structure. The absence of any other discrete peaks confirms the purity of that sample. These results were additionally justified by elemental mapping study (Fig. 4). The corresponding map obtained reveals the compositional elements, i.e., Au, C, N and O species, represented as colored dots, are in excellent homogeneous dispersion all over the surface.

Finally, XRD analysis was used to determine the crystallinity and phase configuration of the CS/NaLS/Au nanocomposite. Single phase of the X-Ray curve affirms the material to be of single and united phase and also highly crystalline in nature. The nature also validates the material is very pure without significant contaminations. Fig. 5 embodies the well-distinguished diffraction peaks observed at $2\theta = 38.7°$, $44.5°$, $66.1°$ and $78.2°$, being attributed to the diffraction on $(1\,1\,1)$, $(2\,0\,0)$, $(2\,2\,0)$ and $(3\,1\,1)$ crystal planes of the Au face centered cubic (*fcc*) crystal (JCPDS No. 65-2870).

3.2. Antioxidant and cytotoxicity effects analysis of CS/NaLS/Au nano bio-composite

Metallic nanoparticles have several compounds, each with a different structure. The extraction of these compounds depends on several factors, the most important of which are the type of solvent and the extraction method. It will be very
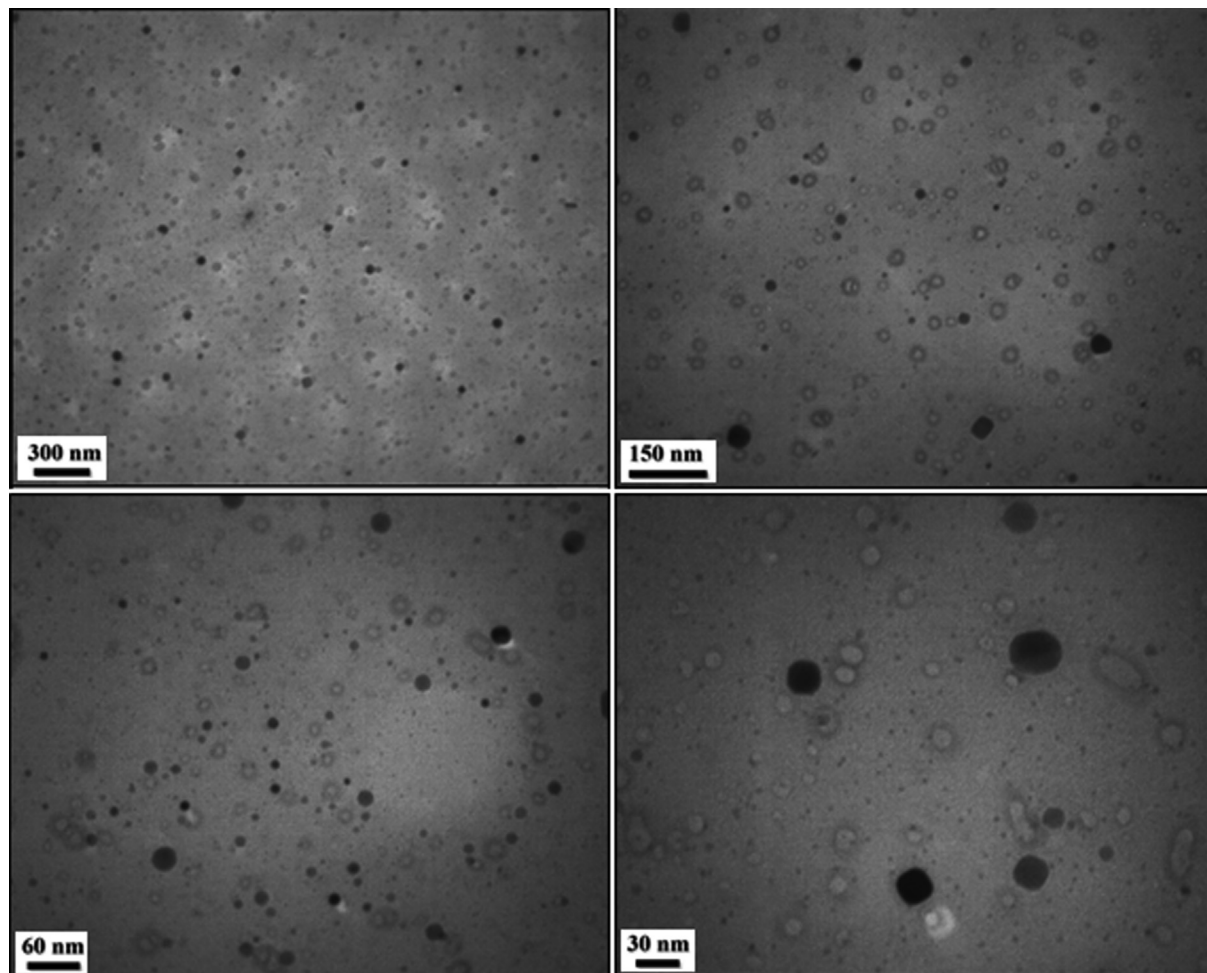

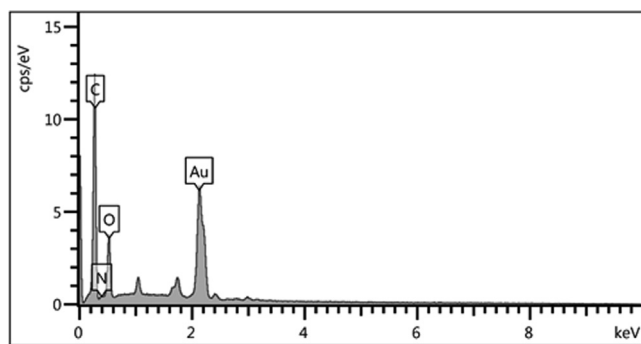**Fig. 2** TEM images of the CS/NaLS/Au nanocomposite.

Fig. 3   EDX spectrum of the CS/NaLS/Au nanocomposite.

difficult to choose a solvent for any group of metallic nanoparticles compounds, because with these compounds, there are other substances that affect the degree of solubility of these substances. When extracting metallic nanoparticles, it should be noted that always use a method that has the best performance in the survival of antioxidant compounds (Namvar et al., 2014; Sankar et al., 2014). Usually metallic nanoparticles have unique antioxidant effects. Recent studies have shown that when these metallic nanoparticles are placed in metal nanoparticles as stabilizing and reducing compounds, they form nanocomposites with extraordinary antioxidant effects. Antioxidants are generally referred to as substances that can delay, slow down, and even stop oxidation processes. These compounds can optimally prevent changes in the color and
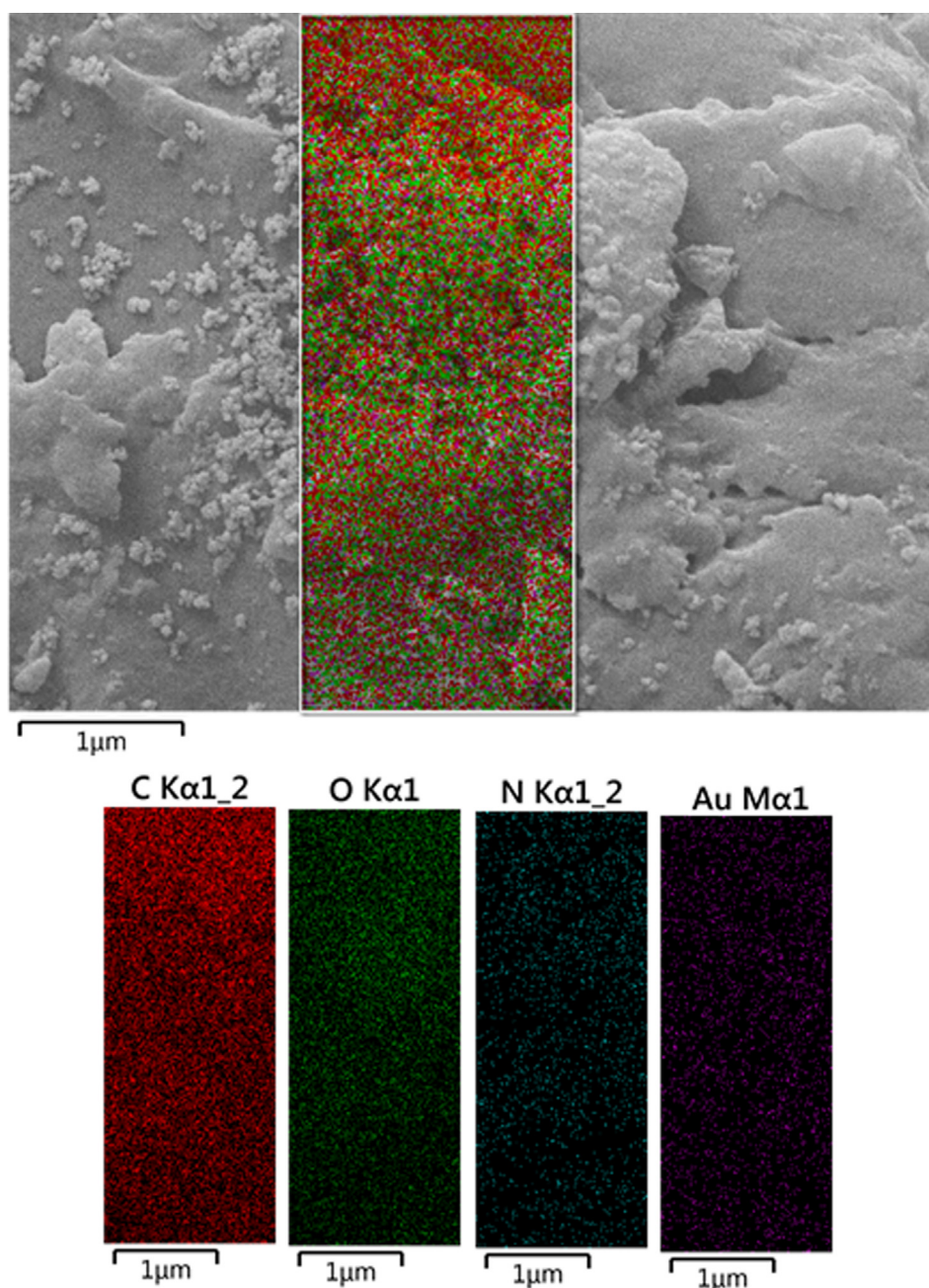

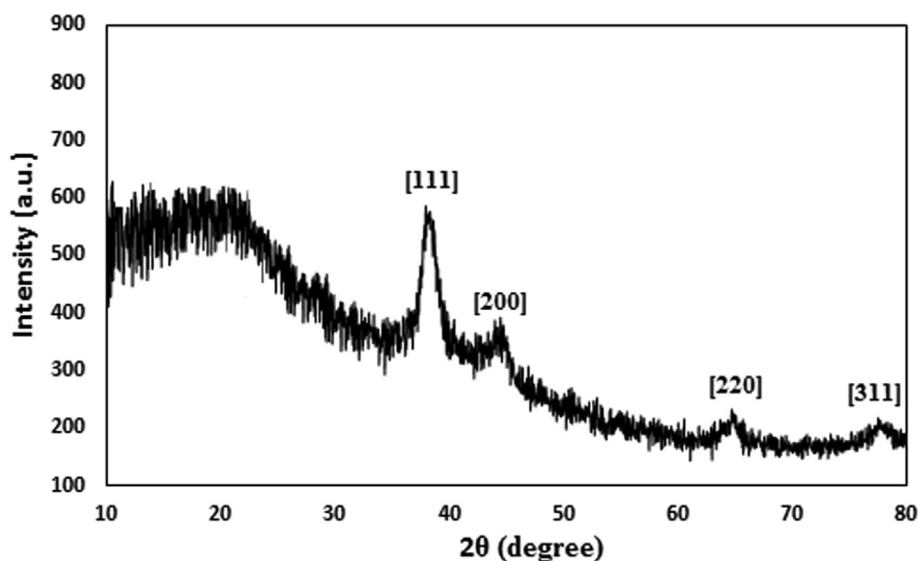**Fig. 4**   Elemental mapping of CS/NaLS/Au nanocomposite.

Fig. 5 XRD pattern of the CS/NaLS/Au nanocomposite.

Table 1 The IC50 of CS/NaLS/Au nano bio-composite and BHT in antioxidant test.

	CS/NaLS/Au nano bio-composite (μg/mL)	BHT (μg/mL)
IC50 against DPPH	117 ± 0[a]	86 ± 0[a]
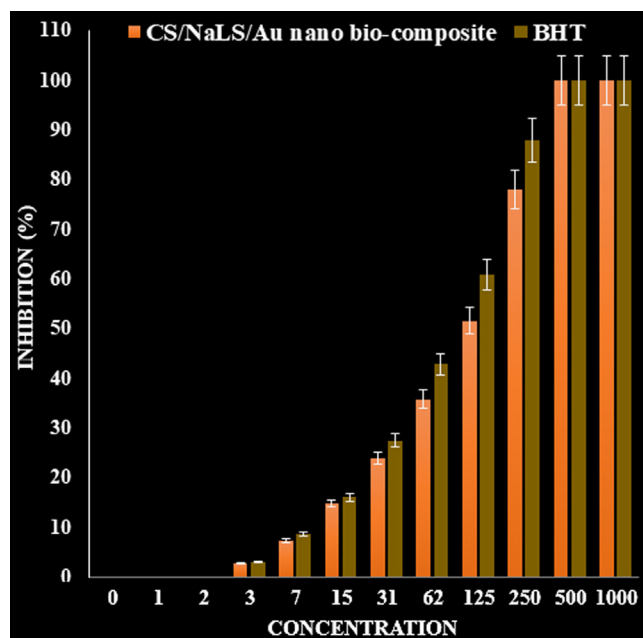
Fig. 6 The antioxidant properties of CS/NaLS/Au nano bio-composite, and BHT against DPPH.

Fig. 7 The cytotoxicity effects of CS/NaLS/Au nano bio-composite against normal cell line.

taste of food because of oxidation reactions (Namvar et al., 2014; Sankar et al., 2014; Katata-Seru et al., 2018; Sangami and Manu, 2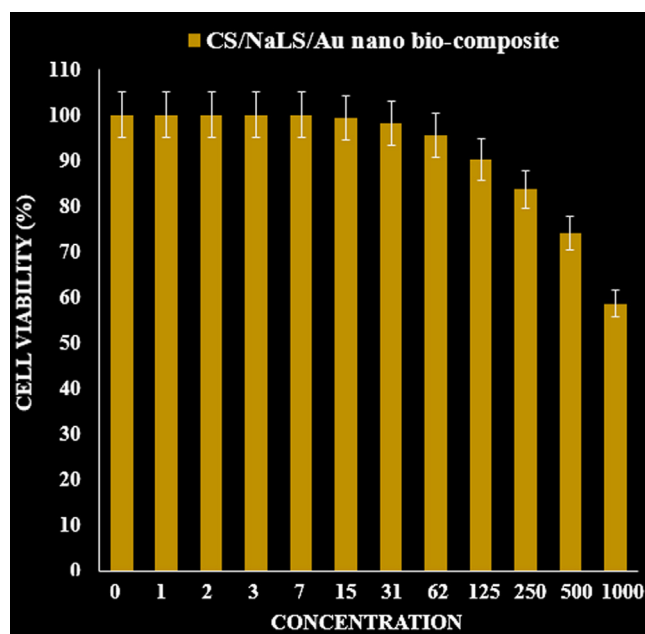017). The antidote to the mechanism of oxidants is that they prevent the spread of oxidation chain reactions by giving hydrogen atoms to free radicals. In recent years, the synthetic antioxidants use such as BHT, BHA, TBHQ as well as other chemical additives has been limited due to their potential toxicity and carcinogenicity. Today, most research in this area focuses on the use of new and safe antioxidants from plant, animal, microbial and food sources (Namvar et al., 2014; Sankar et al., 2014; Katata-Seru et al., 2018; Sangami and Manu, 2017; Beheshtkhoo et al., 2018).

Secondary metabolites in metallic nanoparticles include alkaloids, terpenoids, steroids, saponins, phenols, flavonoids, and amino acids that are used to make various drugs. This trend has paved the way for successful efforts to produce some
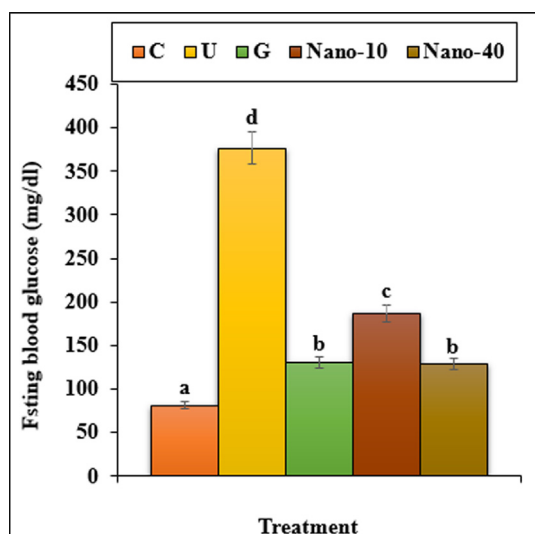
Fig. 8 The fasting blood glucose in the experimental groups. C (Control), U (Untreated diabetic), G (Glibenclamide), Nano (CS/NaLS/Au nano bio-composite). Non-identical letters indicate a significant difference between the groups ($p < 0.05$).

Fig. 10 The absolute volumes of the kidney, cortex and medulla in the experimental groups. C (Control), U (Untreated diabetic), G (Glibenclamide), Nano (CS/NaLS/Au nano bio-composite). Non-identical letters indicate a significant difference between the groups ($p < 0.05$).
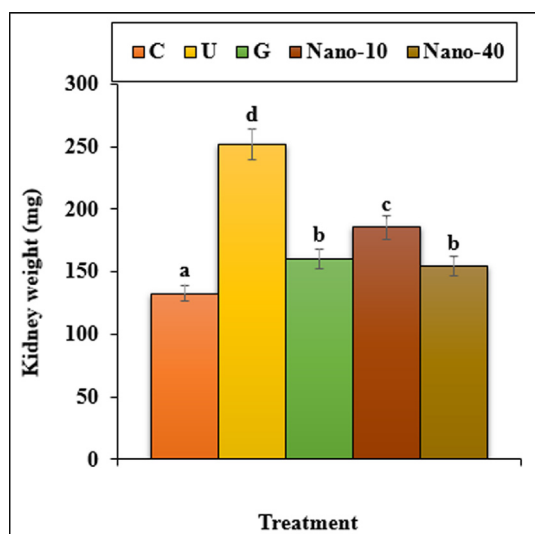

Fig. 9 The weight of kidney in all of the experimental groups. C (Control), U (Untreated diabetic), G (Glibenclamide), Nano (CS/NaLS/Au nano bio-composite). Non-identical letters indicate a significant difference between the groups ($p \leq 0.05$).

valuable drugs (Namvar et al., 2014; Sankar et al., 2014; Katata-Seru et al., 2018). Flavonoids have the structural skeleton of polyphenols or diphenylpropane and consist of two aromatic benzene rings. These compounds are secondary metabolites large family and so far 6000 various flavonoids have been identified. Major flavonoids include compferrol, quercetin, and myristin. The two main flavonoids are luteolin and apigenin, which contain 62 different types found in a variety of vegetables, fruits and edible tropical metallic nanoparticles. Flavonoids have known properties including: removal of free radicals, inhibitors of some enzymes and anti-inflammatory properties (Namvar et al., 2014; Sankar et al.,
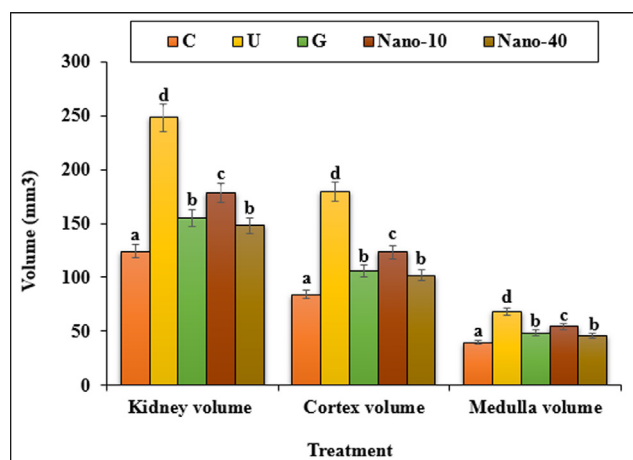
2014; Katata-Seru et al., 2018; Sangami and Manu, 2017). There is some evidence that the biological effects of these compounds are related to their antioxidant activity. Antioxidants work through various mechanisms in the body such as inducing apoptosis, anti-inflammatory effect, immune-boosting effect, cell cycle stopping and cell differentiation (Braendgaard and Gundersen, 1986; Gundersen et al., 1992; Mandarim-de-Lacerda, 2003; Namvar et al., 2014; Sankar et al., 2014; Katata-Seru et al., 2018; Sangami and Manu, 2017; Beheshtkhoo et al., 2018).

In the recent study, the scavenging capacity of CS/NaLS/Au nano bio-composite and BHT at different concentrations expressed as percentage inhibition has been indicated in Table 1 and Fig. 6. In the antioxidant test, the IC50 of CS/NaLS/Au nano bio-composite and BHT against DPPH free radicals were 117 and 86 μg/mL, respectively (Table 1).

In this research, the treated cells with different concentrations of the present CS/NaLS/Au bio-composite were assessed by MTT assay for 48 h about the cytotoxicity properties on normal (HUVEC) cell line (Fig. 7).

3.3. Nephroprotective properties of chitosan/sodium lignosulfonate/Au nanoparticles

The blood glucose concentration enhanced significantly ($p < 0.05$) in untreated-diabetic mice in a time-dependent manner. However, treatment of STZ-diabetic mice with the chitosan/sodium lignosulfonate/Au nanoparticles at 40 dose could significantly ($p < 0.05$) decrease the blood glucose concentration similar to the glibenclamide treated at the end of the experiment. The chitosan/sodium lignosulfonate/Au nanoparticles has the most effect on days 20 of the experiment (Fig. 8).

The results indicated that the weight and volume of kidney and the volumes of cortical and medullary increased ($p < 0.05$) in the untreated mice when compared to the control ones. Administration of chitosan/sodium lignosulfonate/Au nanoparticles and glibenclamide could significantly
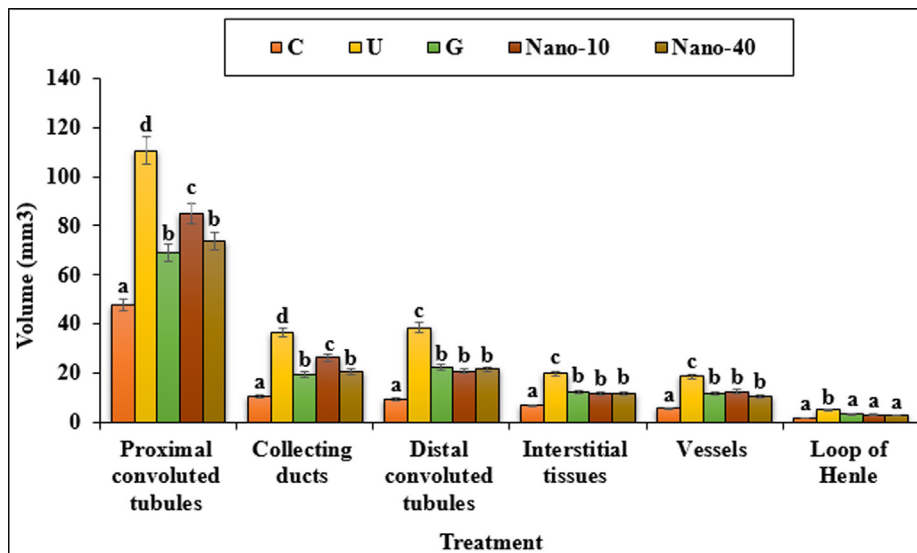
Fig. 11 The absolute volumes of proximal and distal convoluted tubules, collecting ducts, interstitial tissues, vessels and loop of Henle in the experimental groups. C (Control), U (Untreated diabetic), G (Glibenclamide), Nano (CS/NaLS/Au nano bio-composite). Non-identical letters indicate a significant difference between the groups ($p < 0.05$).

Fig. 12 The absolute lengths of the vessels, collecting ducts, proximal and distal convoluted tubules and loop of Henle. C (Control), U (Untreated diabetic), G (Glibenclamide), Nano (CS/NaLS/Au nano bio-composite). Non-identical letters indicate a significant difference between the groups ($p < 0.05$).
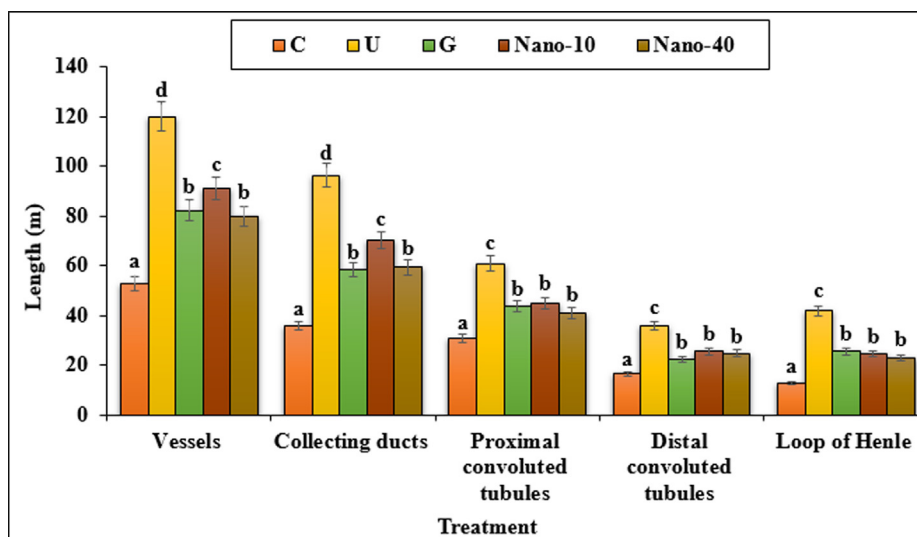
($p < 0.05$) reduce the above parameters when compared to the untreated group (Figs. 9, 10).

The volumes of proximal convoluted tubule, distal convoluted tubule, collecting duct, loop of Henle, vessels and interstitial tissue enhanced significantly ($p < 0.05$) in untreated mice compared to the control ones (Fig. 11). Administration of chitosan/sodium lignosulfonate/Au nanoparticles at both doses and glibenclamide to the mice could significantly ($p < 0.05$) reduce the volumes of the above structures in comparison with the untreated group.

The data of the mean absolute lengths of kidney subcomponents in treated and untreated groups are showed in Fig. 12. Lengths of the proximal convoluted tubule, distal convoluted

tubule, collecting duct, loop of Henle and vessels increased significantly ($p < 0.05$) in untreated mice compared to the control ones. chitosan/sodium lignosulfonate/Au nanoparticles at both doses and glibenclamide could reduce significantly ($p < 0.05$) the lengths of above structures as compared to the untreated group.

The estimated values of the kidney biochemical parameters are presented in Fig. 13. STZ-induced toxicity, increased the concentrations of the urea and creatinine significantly ($p < 0.05$) as compared to the untreated group. Both doses of chitosan/sodium lignosulfonate/Au nanoparticles and glibenclamide could significantly ($p < 0.05$) reduce the above parameters.
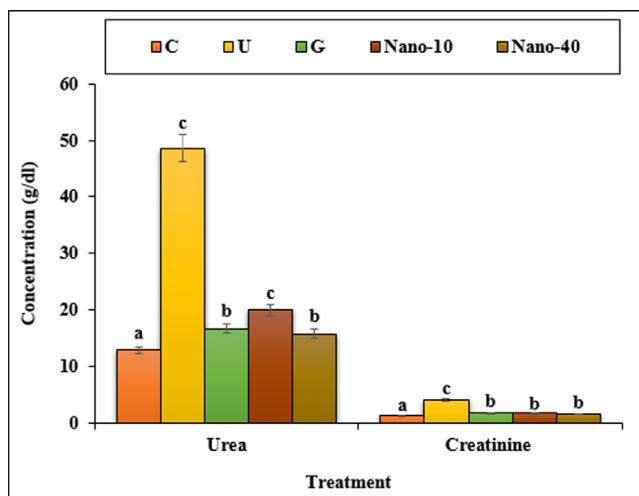
Fig. 13 The levels of urea and creatinine in the experimental groups. C (Control), U (Untreated diabetic), G (Glibenclamide), Nano (CS/NaLS/Au nano bio-composite). Non-identical letters indicate a significant difference between the groups ($p < 0.05$).

4. Conclusion

In conclusion, herein we have demonstrated a unique nanocomposite material with Au NP fabricated over chitosan and sodium ligno-sulphonate combined hydrogel. In the stepwise synthesis Au ions were initially anchored over the pre-formed hydrogel between the two biopolymers and subsequently Au NPs were generated *in situ* by the green rduction over electron rich organofunctions of the gel composite (CS-NaLS). The biomolecular composite provides significant stability to the as synthesized Au NPs by well dispersion as well as capping over the polar functions. The CS/NaLS/Au nanocomposite was analyzed by a wide range of physicochemical techniques. The CS/NaLS/Au nano bio-composite showed the best antioxidant activities against DPPH. The IC50 of CS/NaLS/Au nano bio-composite and BHT against DPPH free radicals were 117 and 86 μg/mL, respectively. In vivo design, CS/NaLS/Au nano bio-composite revealed significant antidiabetic and nephroprotective potentials. This nano bio-composite also demonstrated improvement in histological and biochemical parameters and so might be of value in the treatment of diabetes and nephrotoxicity.

Declaration of Competing Interest

The authors declare that they have no known competing financial interests or personal relationships that could have appeared to influence the work reported in this paper.

References

Aromal, S.A., Philip, D., 2012. Green synthesis of gold nanoparticles using Trigonellafoenum-graecum and its size-dependent catalytic activity. Spectrochim. Acta Part A Mol. Biomol. Spectrosc. 97, 1–5.

Beheshtkhoo, N., Kouhbanani, M.A.J., Savardashtaki, A., et al, 2018. Green synthesis of iron oxide nanoparticles by aqueous leaf extract of Daphne mezereum as a novel dye removing material. Appl. Phys. A 124, 363–369.

Braendgaard, H., Gundersen, H.J., 1986. The impact of recent stereological advances on quantitative studies of the nervous system. J. Neurosci. Methods 18 (1–2), 39–78.

Centers for Disease Control and Prevention, 2011. National diabetes fact sheet: national estimates and general information on diabetes and prediabetes in the United States. US Department of Health and Human Services, Atlanta, GA [accessed September 2, 2014]. Available from: http://www.cdc.gov/diabetes/pubs/pdf/ndfs_2011.pdf.

Debeaufort, F., Quezada-Gallo, J.A., Voilley, A., 1998. Edible films and coatings: tomorrow's packagings: a review. Crit. Rev. Food Sci. 38 (4), 299–313.

Fazaeli, R., Aliyan, H., Fazaeli, N., 2010. Open Catal. J. 3, 14–18.

Fratoddi, I., Cartoni, A., Catone, D., O'Keeffe, P., Paladini, A., Toschi, F., Turchini, S., Sciubba, F., Testa, G., Battocchio, C., Carlini, L., Zaccaria, R.P., Magnano, E., Pis, I., Avaldi, L., 2018. Gold nanoparticles functionalized by rhodamine B isothiocyanate to tune plasmonic effects. J. Colloid Interf. Sci. 513, 10–19.

Gundersen, H.J., Bendtsen, T.F., Korbo, L., Marcussen, N., Møller, A., Nielsen, K., Nyengaard, J.R., Pakkenberg, B., Sorensen, F.B., Vesterby, A., 1992. Some new, simple and efficient stereological methods and their use in pathological research and diagnosis. Acta. Pathol. Microbiol. Immunol. Scand. 96 (5), 379–394.

(a) Hagh-Nazari, L., Goodarzi, N., Zangeneh, M.M., Zangeneh, A., Tahvilian, R., Moradi, R., 2017. Comp. Clin. Path. 26(2), 455-463. (b) Najafi, F., Goodarzi, N., Zangeneh, M.M., Zangeneh, A., Hagh-Nazari, L., 2017. J. Rafsanjan. Univ. Med. Sci. 16(6), 493-504. (c) Zangeneh, M.M., Goodarzi, N., Zangeneh, A., Tahvilian, R., Najafi, F., 2018. Comp Clin Path. 27(4), 861-867. (d) Zangeneh, M.M., Zangeneh, A., Amiri, H., Amiri, N., Tahvilian, R., Moradi, R., Zhaleh, H., Razegh Tehrani, P., 2018. Comp. Cli. Path. 27 (5):1147–1154. (e) Sherkatolabbasieh, H., Hagh-Nazari, L., Shafiezadeh, S., Goodarzi, N., Zangeneh, M.M., Zangeneh, A., 2017. Arch. Biol. Sci. 69(3), 535-543. (f) Farzaei, M.H., Zangeneh, M.M., Goodarzi, N., Zangeneh, A., 2018. Int. J. Morphol. 36(2), 750-757.

Huang, Y., Kang, Y., El-kott, A., Ahmed, A.E., Khames, A., Zein, M.A., 2021. Decorated Cu NPs on Lignin coated magnetic nanoparticles: Its performance in the reduction of nitroarenes and investigation of its anticancer activity in A549 lung cancer cells. Arab. J. Chem. 14, 103299.

International Diabetes Federation, 2013. IDF Diabetes Atlas. 6th ed. International Diabetes Federation, Brussels, Belgium [accessed September 2, 2014]. Available from: http://www.idf.org/sites/default/files/EN_6E_Atlas_Full_0.pdf.

Itani, R., Al Faraj, S.A., 2019. siRNA Conjugated Nanoparticles-A Next Generation Strategy to Treat Lung Cancer. Int. J. Mol. Sci. 20 (23), 6088.

Katata-Seru, L., Moremedi, T., Aremu, O.S., et al, 2018. Green synthesis of iron nanoparticles using Moringa oleifera extracts and their applications: Removal of nitrate from water and antibacterial activity against Escherichia coli. J. Mol. Liq. 256, 296–304.

Ledari, R.T., Zhang, W., Radmanesh, M., Mirmohammadi, S.S., Maleki, A., Cathcart, N., Kitaev, V., 2020. Multi-Stimuli Nanocomposite Therapeutic: Docetaxel Targeted Delivery and Synergies in Treatment of Human Breast Cancer Tumor. Small 16, 2002733.

Lu, Y., Wan, X., Li, L., Sun, P., Liu, G., 2021. Synthesis of a reusable composite of graphene and silver nanoparticles for catalytic reduction of 4- nitrophenol and performance as anti-colorectal carcinoma. J. Mater. Res. Technol. 12, 1832–1843.

Mandarim-de-Lacerda, C.A., 2003. Stereological tools in biomedical research. An. Acad. Bras. Cienc. 75 (4), 469–486.

Miller, K.S., Krochta, J.M., 1997. Oxygen and aroma barrier properties of edible films: a review. Trends Food Sci. Tech. 8 (7), 228–237.

Namvar, F., Rahman, H.S., Mohamad, R., et al, 2014. Cytotoxic effect of magnetic iron oxide nanoparticles synthesized via seaweed aqueous extract. Int. J. Nanomed. 19, 2479–2488.

Oueslati, M.H., Tahar, L.B., Harrath, A.H., 2020. Catalytic, antioxidant and anticancer activities of gold nanoparticles synthesized by

kaempferol glucoside from Lotus leguminosae. Arab. J. Chem. 13, 3112–3122.

Pettitt, D.J., Saad, M.F., Bennett, P.H., Nelson, R.G., Knowler, W.C., 1990. Familial predisposition to renal disease in two generations of Pima Indians with type 2 (non-insulin-dependent) diabetes mellitus. Diabetologia 33 (7), 438–443.

Rossi, A., Donati, S., Fontana, L., Porcaro, F., Battocchio, C., Proietti, E., Venditti, I., Bracci, L., Fratoddi, I., 2016. Negatively charged gold nanoparticles as dexamethasone carrier: stability and cytotoxic activity. RCS Adv. 6, 99016–99022.

Rossing, P., Hougaard, P., Parving, H.H., 2002. Risk factors for development of incipient and overt diabetic nephropathy in type 1 diabetic patients: a 10-year prospective observational study. Diabetes Care 25 (5), 859–864.

Sangami, S., Manu, M., 2017. Synthesis of Green Iron Nanoparticles using Laterite and their application as a Fenton-like catalyst for the degradation of herbicide Ametryn in water. Environ. Technol. Innov. 8, 150–163.

Sankar, R., Maheswari, R., Karthik, S., et al, 2014. Anticancer activity of Ficus religiosa engineered copper oxide nanoparticles. Mat. Sci. Eng. C 44, 234–239.

Satko, S.G., Langefeld, C.D., Daeihagh, P., Bowden, D.W., Rich, S.S., Freedman, B.I., 2002. Nephropathy in siblings of African Americans with overt type 2 diabetic nephropathy. Am. J. Kidney Dis. 40 (3), 489–494.

Scott, L.J., Warram, J.H., Hanna, L.S., Laffel, L.M., Ryan, L., Krolewski, A.S., 2001. A nonlinear effect of hyperglycemia and current cigarette smoking are major determinants of the onset of microalbuminuria in type 1 diabetes. Diabetes 50 (12), 2842–2849.

Seaquist, E.R., Goetz, F.C., Rich, S., Barbosa, J., 1989. Familial clustering of diabetic kidney disease. Evidence for genetic susceptibility to diabetic nephropathy. N. Engl. J. Med. 320 (18), 1161–1165.

Shahriari, M., Sedigh, M.A., Mahdavian, Y., Mahdigholizad, S., Pirhayati, M., Karmakar, B., Veisi, H., 2021. Int. J. Biol. Macromol. 172, 55–65.

Shi, Z., Mahdavian, Y., Mahdavian, Y., Mahdigholizad, S., et al, 2021. Cu immobilized on chitosan-modified iron oxide magnetic nanoparticles: Preparation, characterization and investigation of its anti-lung cancer effects. Arab. J. Chem. 14, 103224.

Singh, P., Pandit, S., Mokkapati, V.R.S.S., Garg, A., Ravikumar, V., Mijakovic, I., 2018. Gold Nanoparticles in Diagnostics and Therapeutics for Human Cancer. Int. J. Mol. Sci. 19, 1979.

Smith, S.R., Svetkey, L.P., Dennis, V.W., 1991. Racial differences in the incidence and progression of renal diseases. Kidney Int. 40 (5), 815–822.

Sun, B., Hu, N., Han, L., Pi, Y., Gao, Y., Chen, K., 2019. Anticancer activity of green synthesised gold nanoparticles from Marsdeniatenacissima inhibits A549 cell proliferation through the apoptotic pathway. Artif. Cell. Nanomed. B. 47, 4012–4019.

Tapp, R.J., Shaw, J.E., Zimmet, P.Z., et al, 2004. Albuminuria is evident in the early stages of diabetes onset: results from the Australian Diabetes, Obesity, and Lifestyle Study (AusDiab). Am. J. Kidney Dis. 44 (5), 792–798.

Torchilin, V.P., 2007. Targeted pharinaceutical nanocarriers for cancer therapy and imaging. AAPS J. 9, E128–E147.

(a) Trojer, M.A., Li, Y., Wallin, M., Holmberg, K., Nyden, M., 2013. Charged microcapsules for controlled release of hydrophobic actives Part II: surface modification by LbL adsorption and lipid bilayer formation on properly anchored dispersant layers. J. Colloid Interface Sci. 409, 8-17; (b) Karimi Ghezeli, Z., Hekmati,

M., Veisi, H., 2019. Synthesis of Imatinib-loaded chitosan-modified magnetic nanoparticles as an anti-cancer agent for pH responsive targeted drug delivery. Appl. Organometallic Chem. 33, e4833; (c) Maleki, B., Hemmati, S., Sedrpoushan, A., Ashrafi, S.S., Veisi, H., 2014. RSC Adv. 4, 40505–40510; (d) Zhang, Wei, Veisi, Hojat, Sharifi, Reyhaneh, Salamat, Delafarin, Karmakar, Bikash, Hekmati, Malak, Hemmati, Saba, Zangeneh, Mohammad Mahdi, Zhang, Zhiyong, Su, Qiang, 2020. Fabrication of Pd NPs on pectin-modified Fe_3O_4 NPs: A magnetically retrievable nanocatalyst for efficient C–C and C–N cross coupling reactions and an investigation of its cardiovascular protective effects. Int. J. Biol. Mac. 160, 1252-1262; (e) Veisi, H., 2010. Synthesis 15, 2631-2635; (f) Taheri, S., Veisi, H., Hekmati, M., 2017. Application of polydopamine sulfamic acid-functionalized magnetic Fe_3O_4 nanoparticles (Fe3O4@PDA-SO3H) as a heterogeneous and recyclable nanocatalyst for the formylation of alcohols and amines under solvent-free conditions. New J. Chem. 41, 5075-5081; (g) Hamelian, M., Varmira, K., Veisi, H., 2018. J. Photochem. Photobiol. B: Biol. 184, 71-79; (h) Veisi, H., Karmakar, B., Tamoradi, T., Hemmati, S., Hekmati, M., Hamelian, M., 2021. Biosynthesis of CuO nanoparticles using aqueous extract of herbal tea (Stachys Lavandulifolia) flowers and evaluation of its catalytic activity, Sci. Rep. 11, 1983; (j) Lotfi, S., Veisi, H., 2019. Mat. Sci. Eng. C 105, 110112.

Umamaheswari, C., Lakshmanan, A., Nagarajan, N.S., 2018. Green synthesis, characterization and catalytic degradation studies of gold nanoparticles against congo red and methyl orange. J. Photochem. Photobiol., B 178, 33–39.

Venditti, I., 2019. Engineered gold-based nanomaterials: morphologies and functionalities in biomedical applications. A mini review. Bioengineering 6 (2), 53–78.

Wu, T., Duan, X., Hu, C., Wu, C., Chen, X., Huang, J., Liu, J., Cui, S., 2018. Synthesis and characterization of gold nanoparticles from Abiesspectabilis extract and its anticancer activity on bladder cancer T24 cells. Artif. Cell. Nanomed. B. 47, 512–523.

Xue, W., Yang, G., Karmakar, B., Gao, Y., 2021. Sustainable synthesis of Cu NPs decorated on pectin modified Fe_3O_4 nanocomposite: Catalytic synthesis of 1-substituted-1H-tetrazoles and invitro studies on its cytotoxicity and anti-colorectal adenocarcinoma effects on HT-29 cell lines. Arab. J. Chem. 14, 103306.

Young, B.A., Maynard, C., Boyko, E.J., 2003. Racial differences in diabetic nephropathy, cardiovascular disease, and mortality in a national population of veterans. Diabetes Care 26 (8), 2392–2399.

Zhaleh, M., Zangeneh, A., Goorani, S., Seydi, N., Zangeneh, M.M., et al, 2019. In vitro and in vivo evaluation of cytotoxicity, antioxidant, antibacterial, antifungal, and cutaneous wound healing properties of gold nanoparticles produced via a green chemistry synthesis using Gundeliatournefortii L. as a capping and reducing agent. Appl. Organometal. Chem. 33, e5015. and references cited therein.

Zhang, W., Veisi, H., Sharifi, R., Salamat, D., Karmakar, B., et al, 2020. Fabrication of Pd NPs on pectin-modified Fe3O4 NPs: A magnetically retrievable nanocatalyst for efficient C-C and C–N cross coupling reactions and an investigation of its cardiovascular protective effects. Int. J. Biol. Macromol. 160, 1252–1262.

Zhao, P., El-kott, A., Ahmed, A.E., Khames, A., Zein, M.A., 2021. Green synthesis of gold nanoparticles (Au NPs) using Tribulus terrestris extract: Investigation of its catalytic activity in the oxidation of sulfides to sulfoxides and study of its anti-acute leukemia activity. Inorg. Chem. Commun. 131, 108781.